Genetic Drift Dominates Genome-Wide Regulatory Evolution Following an Ancient Whole-Genome Duplication in Atlantic Salmon

Jukka-Pekka Verta[1,2,*], Henry J. Barton[1,2], Victoria Pritchard[1,2,3], and Craig R. Primmer[1,2]

[1]Organismal and Evolutionary Biology Research Programme, University of Helsinki, Finland

[2]Institute of Biotechnology, HiLIFE, University of Helsinki, Finland

[3]Present address: Rivers and Lochs Institute, Inverness College, University of the Highlands and Islands, Scotland, United Kingdom

*Corresponding author: E-mail: jukka-pekka.verta@helsinki.fi, jp.verta@gmail.com.

Accepted: 17 March 2021

Abstract

Whole-genome duplications (WGD) have been considered as springboards that potentiate lineage diversification through increasing functional redundancy. Divergence in gene regulatory elements is a central mechanism for evolutionary diversification, yet the patterns and processes governing regulatory divergence following events that lead to massive functional redundancy, such as WGD, remain largely unknown. We studied the patterns of divergence and strength of natural selection on regulatory elements in the Atlantic salmon (*Salmo salar*) genome, which has undergone WGD 100–80 Ma. Using ChIPmentation, we first show that H3K27ac, a histone modification typical to enhancers and promoters, is associated with genic regions, tissue-specific transcription factor binding motifs, and with gene transcription levels in immature testes. Divergence in transcription between duplicated genes from WGD (ohnologs) correlated with difference in the number of proximal regulatory elements, but not with promoter elements, suggesting that functional divergence between ohnologs after WGD is mainly driven by enhancers. By comparing H3K27ac regions between duplicated genome blocks, we further show that a longer polyploid state post-WGD has constrained regulatory divergence. Patterns of genetic diversity across natural populations inferred from resequencing indicate that recent evolutionary pressures on H3K27ac regions are dominated by largely neutral evolution. In sum, our results suggest that post-WGD functional redundancy in regulatory elements continues to have an impact on the evolution of the salmon genome, promoting largely neutral evolution of regulatory elements despite their association with transcription levels. These results highlight a case where genome-wide regulatory evolution following an ancient WGD is dominated by genetic drift.

Key words: whole-genome duplication, ChIPmentation, gene regulation, distribution of fitness effects, Atlantic salmon, histone acetylation.

Significance

Regulatory evolution following whole-genome duplications (WGD) has been investigated at the gene expression level, but studies of the regulatory elements that control expression have been lacking. By investigating regulatory elements in the Atlantic salmon genome, which has undergone a whole-genome duplication 100–80 Ma, we discovered patterns suggesting that neutral divergence is the prevalent mode of regulatory element evolution post-WGD. Our results suggest mechanisms for explaining the prevalence of asymmetric gene expression evolution following whole-genome duplication, as well as the mismatch between evolutionary rates in enhancers versus that of promoters.

Introduction

Numerous evolutionary innovations have taken place in conjunction with, or following, large-scale genomic rearrangements such as whole-genome duplications (WGD) (Vandepoele et al. 2004; Peer et al. 2009; Macqueen and Johnston 2014), which create massive functional redundancy of genes and regulatory elements. The effects of increased functional redundancy are thought to reflect onto gene expression evolution, albeit being varied and contingent on the function of the genes impacted (Robertson et al. 2017; Hallin and Landry 2019). Yet, the impacts of whole-genome duplications on patterns of regulatory divergence and evolutionary forces acting on regulatory elements remain poorly documented and understood.

Gene expression levels and patterns in metazoan genomes are controlled by enhancer and promoter sequences commonly referred to as regulatory elements (Long et al. 2016). Regulatory elements contain recognition motifs for transcription factors (TFs) that cooperatively orchestrate gene expression of their target genes. Regulation of mammalian gene expression is putatively controlled by hundreds of thousands of regulatory elements (Villar et al. 2014; Gasperini et al. 2020), their number greatly exceeding the typical number of genes. Through their combined and individual function, regulatory elements have long been hypothesized to significantly contribute to evolutionary change and adaptation (King and Wilson 1975; Stern and Orgogozo 2008).

Gene regulatory elements can be mapped genome-wide by their distinct chromatin structure without knowledge of the specific TFs that recognize each element (Andersson and Sandelin 2019). Chromatin immunoprecipitation followed by high throughput sequencing (ChIP-seq) of H3K27 acetylation (H3K27ac), an epigenetic mark associated with active enhancers and promoters (Creyghton et al. 2010), has been particularly informative for studies on the evolution of regulatory elements. Widely applicable ChIP-seq strategies for H3K27ac have facilitated studies on the evolution of regulatory elements across species, revealing that enhancers in particular can evolve rapidly (Villar et al. 2015). However, little is known about how features of genome evolution such as prolonged polyploid history following WGD influences regulatory evolution (Elurbe et al. 2017). Studying regulatory element evolution in post-WGD genomes is essential for a more comprehensive understanding how functional redundancy impacts regulatory evolution and species diversity.

Salmonid fishes are a promising system for studying regulatory evolution in post-WGD genomes. Salmonids underwent a WGD 100–80 Ma, which is considerably more recent compared to the more commonly studied mammals (that share a WGD at the base of the vertebrate tree approximately 500 Ma; Dehal and Boore 2005; Sacerdot et al. 2018). The salmonid genome duplication resulted in a portion of the genome remaining in effective polyploidy (Lien et al. 2016). Despite massive gene and functional redundancy still existing in salmonid genomes, most gene duplicates from WGD (hereafter ohnologs, called homeologs in Lien et al. [2016] or WGD paralogs) can be confidently identified, facilitating broad-scale genomic studies of ohnolog duplicate pairs. Across salmonids, gene expression evolution is dominated by asymmetric evolution where ohnologs retain and lose expression patterns in an unbalanced pattern (Lien et al. 2016; Gillard et al. 2020). Asymmetric expression evolution of ohnologs suggests that expression changes are driven by divergence in *cis*-acting regulatory elements such as enhancers and promoters because both gene copies are exposed to the same *trans*-acting factors within a cell. Studying evolutionary dynamics in gene regulatory regions however requires a map of enhancer and promoter elements.

Here, we studied gene regulatory elements in Atlantic salmon (*Salmo salar*). By mapping regulatory elements in the tissue with the most transcribed genes, the testis, we characterized the association of H3K27ac with gene transcription and the presence of transcription factor recognition motifs. We compared regulatory elements between ohnologs and large-scale duplicate regions called homeoblocks, and discovered patterns consistent with large-scale, neutral divergence of regulatory elements. We further modeled the current strength of selection on regulatory elements using population resequencing data to show that regulatory elements continue to experience predominantly neutral evolution. Our results point toward a pattern of largely neutral regulatory element evolution within this post-WGD genome.

Results

H3K27ac ChIPmentation Peaks Associate with Gene Regions

To address the paucity of regulatory element genetic maps in species with recently duplicated genomes, we used ChIPmentation (Schmidl et al. 2015) of H3K27ac in immature salmon testis to map putative regulatory regions of the Atlantic salmon genome. Immature testes express the broadest number of salmon transcripts among 14 tested tissues (supplementary fig. S1, Supplementary Material online), making testis well-suited for inferring regulatory regions in a genome-wide manner using a single tissue. Our analysis detected 34,489 reproducible H3K27ac regions (hereafter "peaks," $\mathrm{FDR} < 0.05$ and $\log\mathrm{FC} > 1$, $N = 5$, fig. 1*A*). H3K27ac peak widths formed a marked periodical pattern with a median size of 623 bp, supporting the peaks corresponding to sets of nucleosomes with acetylated histones (supplementary fig. S2, Supplementary Material online).

Regions containing genes showed a distinctive pattern of high H3K27ac signal, consistent with a highly organized nucleosome occupancy (Mavrich et al. 2008; Jiang and Pugh 2009). Strikingly, such organized nucleosome occupancy

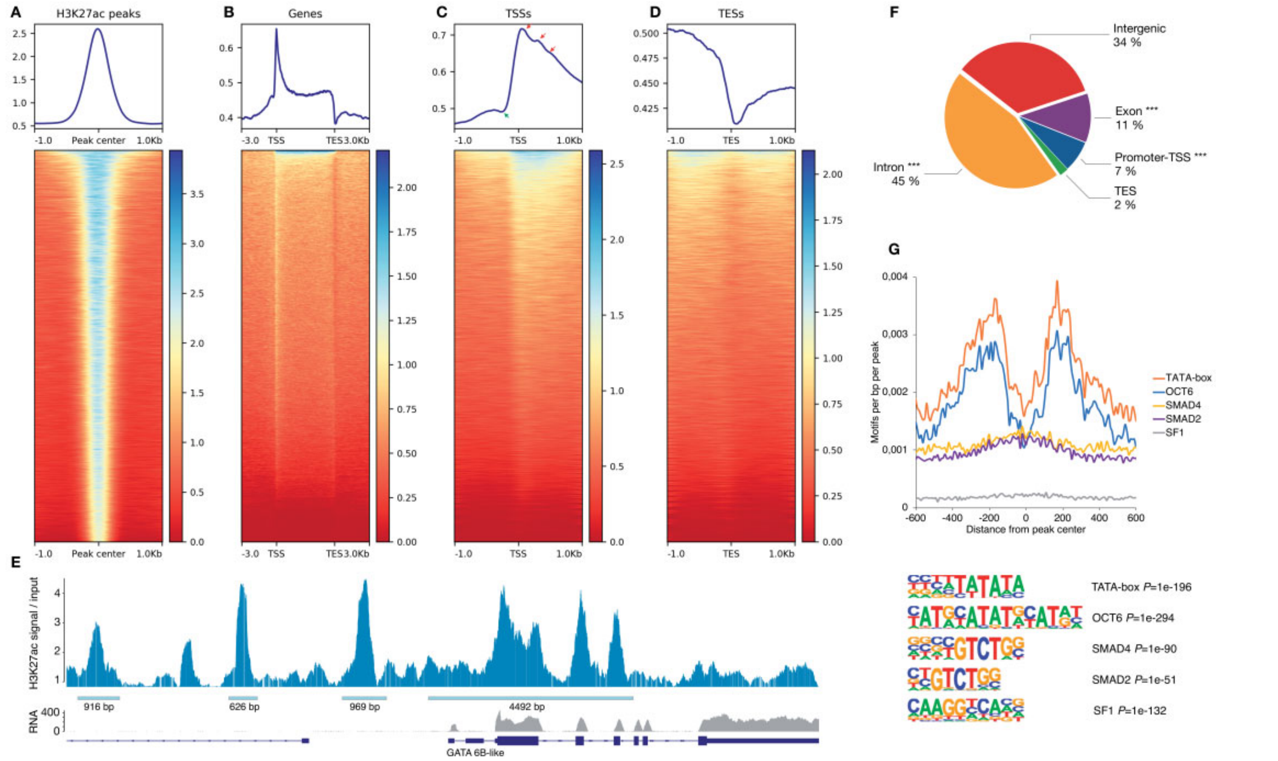

Fig. 1.—Key features of Atlantic salmon H3K27ac regions and associated genes in testis. (*A*) H3K27ac ChIPmentation signal over replicated H3K27ac peaks. (*B*) The majority of 81,586 inferred salmon genes show increased H3K27ac signal (including protein-coding and noncoding genes). (*C*) Transcription start sites (TSS) show particularly high H3K27ac signal with a prominent nucleosome depleted region (NDR) immediately upstream of TSS (green arrow). Red arrows correspond to +1, +2, and +3 nucleosomes. (*D*) Transcription end sites (TES) are characterized by a prominent NDR. (*E*) A region with prominent H3K27ac peaks overlapping the *GATA 6B-like* locus. (*F*) Division of 34,489 reproducible H3K27ac peaks according to genomic feature type. ***, likelihood-ratio overrepresentation $P < 0.001$. (*G*) Density of six testis cell-type associated and overrepresented TF motifs relative to H3K27ac peak center (upper panel). Motif sequences of TF motifs with their overrepresentation *P* values (lower panel).

was observed for the majority of the 81,586 protein coding and non-coding salmon genes inferred (fig. 1*B*), consistent with broad expression of genes in the testes. Transcription start site (TSS) regions were characterized by a dip in H3K27ac signal immediately upstream of the TSS corresponding to the 5′ nucleosome depleted region (NDR) observed in expressed genes (fig. 1*C* green arrow). Nucleosome patterning with acetylated H3K27 could also be observed for the three nucleosomes downstream from the TSS, with strongest signal on the first (+1) nucleosome (fig. 1*C* red arrows). Transcription end sites (TES) were characterized by a 3′ NDR void of H3K27ac signal, corresponding to the region of transcription termination (fig. 1*D*). The largest single H3K27ac region, comprising of multiple individual H3K27ac peaks, overlapped with *GATA 6B-like* gene locus (fig. 1*E*), which is expressed in Sertoli and germ cells, and plays a central and conserved role in regulating testis gene expression and cell differentiation (Viger et al. 2008).

Overall, the distribution of H3K27ac peaks showed association with promoters (defined as −1,000 to +100 bp from TSS), exons (including the 5′-UTR), and especially introns, which contained the largest percentage, 45%, of the peaks (fig. 1*F*). We further used a set of peaks with 500 bp width and centered to nucleosome depleted regions to identify overrepresented motifs in H3K27ac peaks. These replicated peaks overlapped 83% of the original peak set and were overrepresented in motifs for general promoter features (TATA-box 26.8% of peaks), as well as for transcription factors implicated in the development of spermatogonia (*OCT6* 10.5% of peaks), Sertoli and Leydig cells (*SMAD4* 41% of peaks, *SMAD2* 38.4% of peaks, *FoxL2* 36.7% of peaks, *SF1* 9.3% of peaks, and *SMAD3* 2.3% of peaks). Plotting motif density relative to peak center revealed that TATA, *OCT6*, and *FoxL2* motifs tended to be situated 200 base pairs to the left and right of peak center, whereas *SMAD* and SF1 motifs were centered on peaks (fig. 1*G*). We hypothesize that this pattern can arise from the latter two motifs residing primarily in proximity to regions with well-defined NDR such as TSSs. Genes proximal to at least one H3K27ac peak ($N = 40,232$) were enriched for two GO functions notably involved in cell signaling and differentiation ("transmembrane receptor protein kinase activity" $P < 2.74\text{e-}05$ and "steroid hormone receptor activity" $P < 2.74\text{e-}05$), consistent with precise regulation of cell cycle in immature testis cell types. Together these data

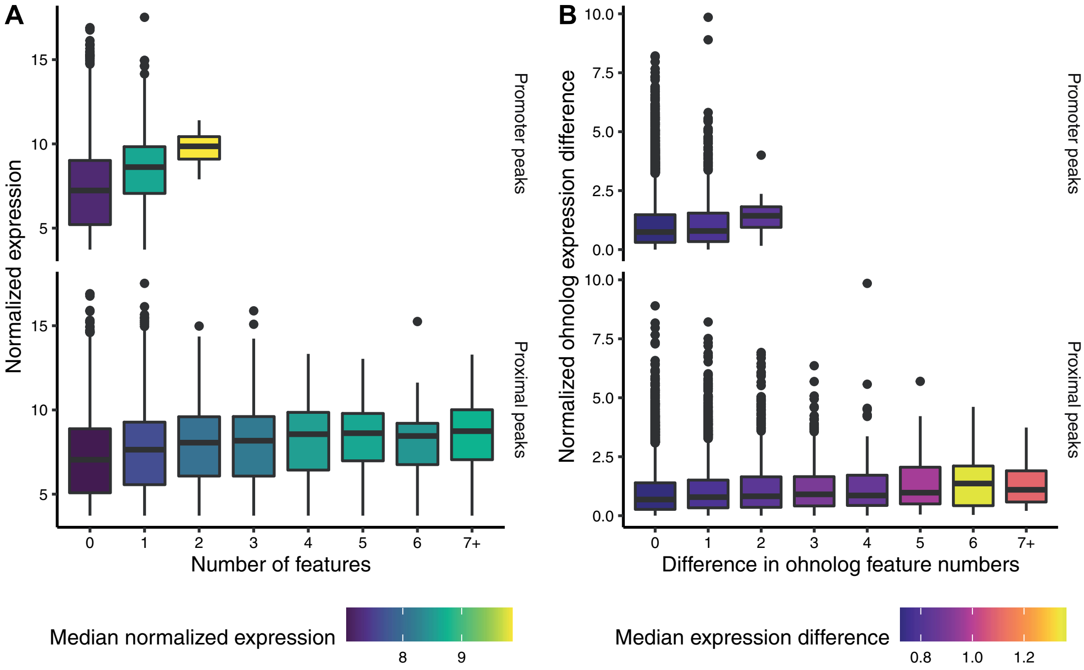

Fig. 2.—H3K27ac peaks are associated with gene expression levels. (*A*) Number of promoter and proximal peaks correlates positively with gene expression levels in testis. (*B*) Difference in proximal peaks, but not promoter peaks, correlates with expression differences between ohnologs from WGD.

demonstrate that H3K27ac regions in Atlantic salmon testis bear the hallmarks of actively transcribed genes and tissue-specific regulation of cell type differentiation.

Divergence in Proximal Peaks Tracks Expression Divergence between Ohnologs

To further determine whether the H3K27ac peaks were associated with regulatory activity, and therefore represented true gene regulatory elements, we investigated peaks in conjunction with expression levels of genes in immature testis RNA-seq data. We hypothesized that if H3K27ac peaks functioned in an additive manner, the number of peaks assigned to genes should correlate with their expression levels. Indeed, the number of peaks assigned to gene promoters (−1,000 to +100 bp relative to TSSs), and all other proximal peaks (all peaks except promoter peaks) assigned to nearest TSSs (supplementary fig. S3, Supplementary Material online) correlated positively with immature testis gene expression levels (Spearman's rho = 0.09, linear regression $P < 2.2\text{e-}16$ and rho = 0.12, $P < 2.2\text{e-}16$, for promoter and proximal peaks, respectively) (fig. 2*A*). These results support the H3K27ac regions being functional promoter and enhancer elements with an additive effect on expression levels of proximal genes.

We next investigated whether divergence in H3K27ac peaks between ohnologs from WGD had phenotypic impacts by comparing the number of assigned peaks and the expression levels between ohnologs. The number of peaks assigned to one ohnolog could not be used to predict the number of peaks assigned to the other (supplementary fig. S4, Supplementary Material online), with the exception of rare ohnolog pairs with one promoter H3K27ac peak each ($N = 73$, hypergeometric test $P < 5.51\text{e-}21$), indicating a general absence of conservation for the number of regulatory elements for ohnologs. These results were robust to different strategies for identifying ohnologs (supplementary analysis, Supplementary Material online).

To test whether the observed differences in the number of peaks assigned to ohnologs had phenotypic effects, we compared the difference in peak number to expression differences between the ohnologs. Divergence in proximal peak number was positively associated with divergence in mean expression levels (linear regression $P < 2.2\text{e-}16$, fig. 2*B*), whereas the difference in only promoter peaks did not predict expression difference (linear regression $P < 0.072$, fig. 2*B*). These results indicate that the number of peaks assigned to ohnologs seems to diverge in a random fashion, yet divergence in proximal H3K27ac peaks between ohnologs has a phenotypic impact of increasing the level of expression differences.

Reploidization Age of Homeoblocks Predicts the Magnitude of Divergence in the Regulatory Landscape

Whole-genome duplications can leave large portions of the genome remaining in effective polyploidy until recent evolutionary history (Lien et al. 2016), yet the extent to which

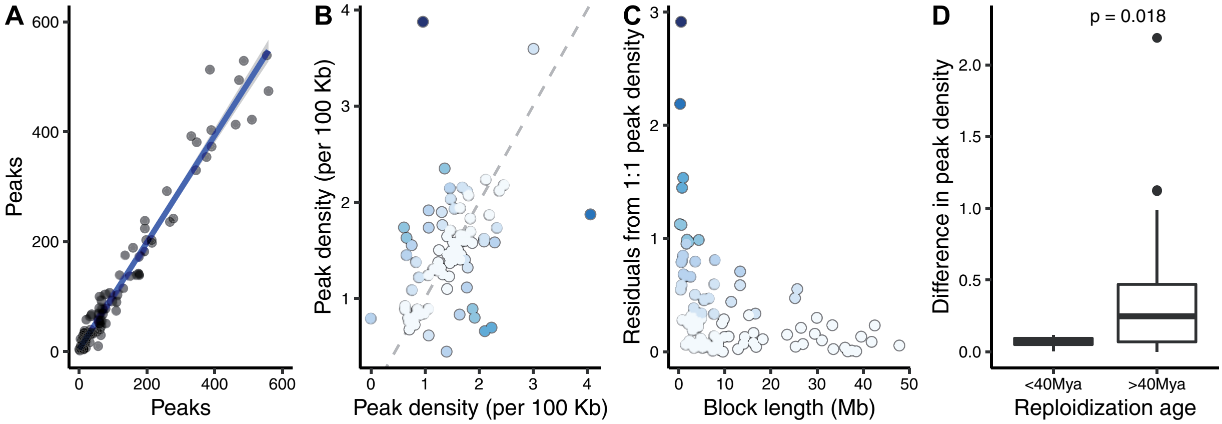

FIG. 3.—Comparison of H3K27ac peaks between homeoblocks from WGD. (*A*) The number of H3K27ac peaks is highly correlated between homeoblocks. (*B*) Peak density identifies homeoblocks that have diverged more from the expected 1:1 density (grey dashed line). Points are colored for residuals from 1:1 line. (*C*) Peak density has diverged more in homeoblocks with shorter length. (*D*) Homeoblocks that have remained in effective polyploidy until more recently have diverged less in peak density.

duplicated genome regions share, or differ in, regulatory elements remain unknown. To investigate the large-scale trends in regulatory element evolution between duplicated genome regions from WGD, we first compared H3K27ac peaks assigned to homeoblocks. Overall, H3K27ac peak numbers were highly correlated between homeoblocks (linear regression $R^2 = 0.98$, $P < 2.2\text{e-}16$, fig. 3*A*). Normalizing the number of H3K27ac peaks to the length of the homeoblocks revealed divergence from the equal H3K27ac peak density between blocks (fig. 3*B*). Difference from equal peak density followed block length in a manner where shorter homeoblocks were diverged more in peak density compared to longer homeoblocks (fig. 3*C*).

The Atlantic salmon genome contains regions that have remained polyploid until as recently as 40 Ma, and which have been proposed to be implicated in salmonid adaptations (Robertson et al. 2017). Therefore, we tested whether the time since reploidization of homeoblocks as defined in Lien et al. (2016) influenced divergence in regulatory region density. Homeoblocks with reploidization age less than 40 Ma were significantly more conserved in H3K27ac peak density ($P = 0.018$, fig. 3*D*), suggesting that a longer polyploid state of homeoblocks has constrained asymmetric regulatory divergence between the blocks.

We next investigated the genomic distribution of H3K27ac peaks to understand whether certain regions of the genome showed higher peak densities or differences therein. All chromosomes showed regulatory region activity (supplementary fig. S5, Supplementary Material online), and overall, the number of peaks in 10-Mb bins along chromosomes was correlated to the number of expressed genes in the same bins ($R^2 = 0.2$, linear regression $P < 1.3\text{e-}13$, supplementary fig. S6, Supplementary Material online). There were also indications that homeoblocks with most elevated differences in H3K27ac density per 100 kb of block length tended to group to certain chromosomes. Notably, chromosome 19 contained three of the ten blocks with the most diverged peak density (hypergeometric test $P < 0.012$, supplementary fig. S5*A*, Supplementary Material online), followed by chromosome 1 containing four (hypergeometric test $P < 0.018$, supplementary fig. S5*A*, Supplementary Material online), and chromosome 9 containing three (hypergeometric test $P < 0.012$, supplementary fig. S5*A*, Supplementary Material online) (each block is present in two genome locations by definition). The ten most diverged homeoblocks accounted for an approximate length of 26.44 Mb of the 2.13 Gb assigned to homeoblocks, indicating that extreme regulatory divergence between homeoblocks, although overrepresented in certain chromosomes, impacts a minority of the genome.

Largely Neutral Evolution of Functional Elements in Natural Populations

To better understand the evolution of regulatory elements in Atlantic salmon populations across Northern Europe that had been established since the last glaciation 10,000 years ago, we analyzed a population resequencing data set comprised of 31 salmon individuals (Barson et al. 2015). All H3K27ac peaks combined showed comparable Tajima's *D* and π estimates to putatively neutral 4-fold degenerate sites (fig. 4). When compared to their sequence context, H3K27ac peaks were generally not different from the whole genome. Nucleotide diversity was more strongly reduced in sequence contexts expected to be under stronger purifying selection, with the following order from highest to lowest diversity: introns, intergenic regions, UTRs, CDS regions, and 0-fold degenerate sites, respectively (fig. 4). The exception to this were H3K27ac peaks assigned to intronic and intergenic regions that had significantly elevated π (bootstrapping $P < 0.05$) compared with the regions as a whole. However, these

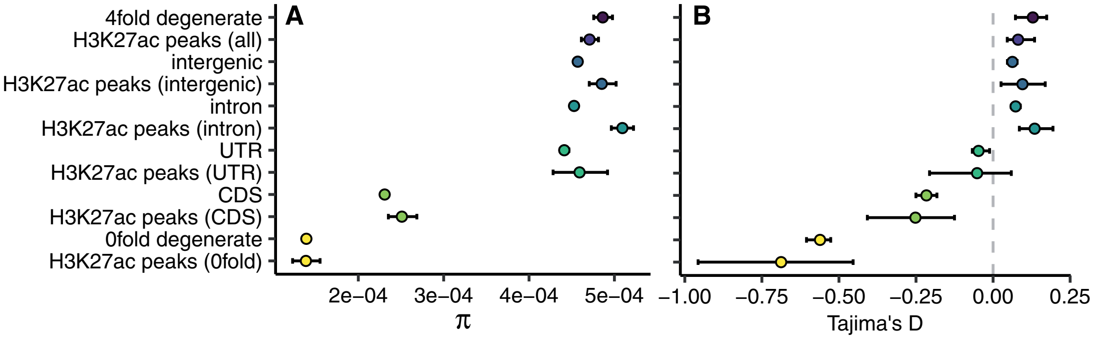

FIG. 4.—Population genetic summary statistics for H3K27ac peaks reflect their genomic location. (*A*) Nucleotide diversity (π) and (*B*) Tajima's *D* estimates for all genomic regions and H3K27ac peaks. Values were estimated for SNPs in the following categories: 4-fold degenerate (putatively neutral), intergenic, intronic, untranslated region (UTR), coding sequence (CDS), and 0-fold degenerate sites, as well as all SNPs falling within those regions and within identified H3K27ac peaks. Error bars represent 95% confidence intervals obtained from 100 rounds of bootstrapping by gene.

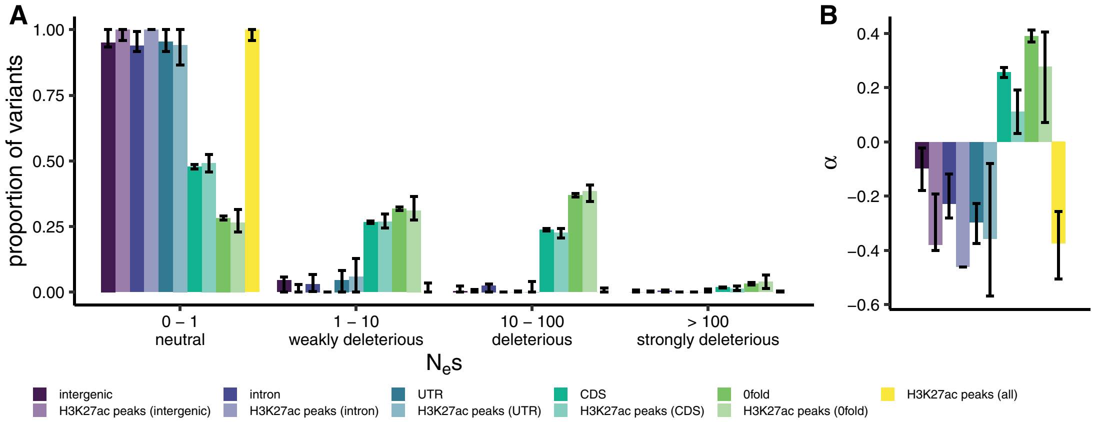

FIG. 5.—The DFE and α for H3K27ac peaks support predominantly neutral evolution. Estimated distribution of fitness effects of new mutations (*A*; DFE) and the proportion of substitutions fixed by positive selection (*B*; α) in different genomic regions and H3K27ac peaks in those regions, using the population resequencing data set. The DFE is presented as the proportion of variants falling into four selective bins: effectively neutral ($0 \leqslant N_e s \leqslant 1$), weakly deleterious ($1 < N_e s \leqslant 10$), deleterious ($10 < N_e s \leqslant 100$), and strongly deleterious ($N_e s > 100$). Error bars represent 95% confidence intervals obtained from 100 rounds of bootstrapping by gene.

H3K27ac regions did not significantly differ from π at 4-fold degenerate sites. Additionally, Tajima's *D* at intronic and intergenic H3K27ac peaks was not significantly different from *D* at 4-fold degenerate sites.

To further quantify the selective pressures in H3K27ac peaks while controlling for the confounding effects of demography, we obtained maximum likelihood estimates of the distribution of fitness effects of new mutations (DFE). For intergenic regions, introns, UTRs, H3K27ac peaks within these regions, and all H3K27ac peaks combined, we estimated that the majority of point mutations have $N_e s \leqslant 1$ (fig. 5*A*), suggesting that these regions are evolving neutrally. We additionally used the DFE to calculate the fixation probability of deleterious mutations and consequently the proportion of substitutions fixed by positive selection (α). Slightly negative α values for these regions provided no evidence of positive selection (fig. 5*B*).

The exception to the predominantly neutral pattern of genetic variation was CDS regions and 0-fold degenerate sites, and the H3K27ac peaks therein. These regions were more enriched for SNPs in the weakly deleterious, deleterious, and strongly deleterious categories (fig. 5*A*). Estimates of α in CDS and 0-fold degenerate sites indicated the presence of adaptive substitutions at these sites, not seen in other sequence categories (fig. 5*B*). We observed a significantly lower α of 0.11 at CDS H3K27ac peaks than at CDS sites as a whole (bootstrapping $P < 0.05$), but no significant difference between 0-fold degenerate H3K27ac peak sites and 0-fold degenerate sites in general (fig. 5*B*).

Discussion

Molecular evolutionary processes, including the evolution of gene regulatory elements, have remained poorly understood in genomes that contain massive functional redundancy (Elurbe et al. 2017). Analysis of modern genomes derived from whole-genome duplications (WGD) can yield critical insights into regulatory evolution after WGD, specifically pertaining to questions such as the extent and tempo of divergence in regulatory elements between duplicate genome regions, level of regulatory conservation between duplicated genes, and selective forces on regulatory elements. To address these knowledge gaps, we mapped regulatory elements in the Atlantic salmon genome by means of H3K27ac ChIPmentation and analysis of RNA-seq data, and examined contemporary selection forces on regulatory elements by population resequencing.

Mapping of histone modifications through ChIP-seq has been established as a powerful method for inferring putative regulatory elements in metazoan genomes (Andersson and Sandelin 2019). Being dispersed over multiple nucleosomes bordering regulatory elements has in some cases hindered the resolution of histone ChIP-seq signal, and multiple variants of the technique have been developed to yield greater resolution (Skene and Henikoff 2015). By using a ChIPmentation strategy that implements Tn5-mediated integration of sequencing adapters to a conventional ChIP-seq protocol (Schmidl et al. 2015), our results suggest that acetylated histones can be mapped with near-nucleosome precision in Atlantic salmon using our adapted protocol that is suitable for very small samples. Notably, H3K27ac signal around Atlantic salmon genes showed a distinctive nucleosome patterning with -1, $+1$, $+2$, and $+3$ acetylated nucleosome bordering transcription start sites, as well as distinctive nucleosome depleted regions immediately upstream of transcription start and downstream of transcription termination sites. These features are a conserved mechanism associated with active transcription (Jiang and Pugh 2009).

We further show an association between H3K27ac peaks and general transcriptional motifs, such as TATA-box, as well as transcription factor motifs such as *OCT6* (*Pou3f1*), *SMADs*, *SF1*, and *FoxL2*. These transcription factors have broadly conserved roles in sexual development. *OCT6* is known to be expressed in murine testes and to regulate spermatogonial germ cell renewal (Wu et al. 2010) but to our knowledge has not previously been implicated in fish testis development. *SMADs* and *SF1* are key regulators of testicular cell type differentiation in fish (Sandra and Norma 2010; Pfennig et al. 2015). Notably, the overrepresentation of *SMAD2* and *SMAD3* motifs in H3K27ac peaks highlights the importance of the transforming growth factor β (TGF-β) and activin pathways in regulating immature testis differentiation. We also observed an overrepresentation of *FoxL2* motifs (supplementary analysis, Supplementary Material online), supporting that this transcription factor, most often associated with teleost ovary development, may play a role in male gonad development as well (Baron et al. 2005; Liu et al. 2007). Taken together, we anticipate that further assessment of ChIPmentation with additional tissues, epigenetic modifications, as well as transcription factors, will greatly accelerate the functional annotation of salmonid genomes (Macqueen et al. 2017).

Leveraging on reproducible H3K27ac peaks and publicly available RNA-seq data, we investigated the functional effect that divergence in regulatory elements imparts on gene expression levels between ohnologs. We observed that ohnolog expression divergence was predicted by the difference in the number of proximal peaks assigned to each ohnolog (putative enhancer elements), but not by the difference in peaks assigned to promoter regions (putative promoter elements). Our observations may reflect the lower number of differences in promoter peaks, and hence lower statistical power, but could also have a biological basis in the function of enhancer and promoter elements. Enhancers can act over large genomic distances (Long et al. 2016) and do not necessarily regulate the closest gene (Cao et al. 2017). Enhancers and promoters evolve at different rates across mammals, where divergence in promoters is notably slower (Villar et al. 2015). Interestingly, (Berthelot et al. 2018) observed a switch-like behavior for promoters, where one promoter element was enough to activate expression and additional promoter elements did not correlate with expression level increase. In contrast, our data show that an increase in promoter peaks correlates with higher expression. Increase in promoter peaks did not however correlate with expression difference between ohnologs, suggesting that divergence in enhancer elements is the primary mechanism for ohnolog expression divergence after WGD.

Genomes from WGD contain duplicated chromosomes that break down into smaller segments, called homeoblocks, over time due to recombination and structural changes. Homeoblocks are known to harbor functional ohnolog genes, yet until now the level and pattern of regulatory element conservation in homeoblocks has remained unclear. By comparing regulatory evolution at the homeoblock level, we observed that differences in H3K27ac peaks normalized to homeoblock length (i.e., peak density) were stronger in shorter homeoblocks. These results may suggest that differences in H3K27ac peaks between homeoblocks are largely a product of random loss or gain in peaks, whereby stochastic processes lead to a larger impact on peak density per unit of block in shorter homeoblocks. Not all regulatory regions of the Atlantic salmon genome evolve at the same rate; retention of polyploid state for a longer period correlated with less regulatory divergence (slower regulatory evolution) between homeoblocks. These results are consistent with lower levels of expression divergence between ohnologs residing in regions with longer polyploid history (Robertson et al. 2017). Longer retained polyploid state also correlated with higher sequence similarity (Lien et al. 2016), which may explain why these regulatory regions show higher conservation in H3K27ac peak densities. It is also worth noting that, in regions with longer polyploid state, speciation has preceded ohnolog divergence (Robertson et al. 2017); ohnologs residing in these regions have diverged independently within salmonid species and are therefore good candidates for contributing to species-specific adaptations. Overall, our results paint a picture which is compatible with massive post-WGD functional redundancy leading to predominantly neutral divergence of regulatory elements between duplicated genome regions, with more restrained evolution in recently polyploid genome regions possibly indicating stronger selection.

Neutral regulatory evolution stemming from functional redundancy is seemingly in contrast with our results that divergence in regulatory elements correlated with phenotypic divergence between ohnologs. Reconciling random regulatory divergence between ohnologs and the functional effects of such evolution requires understanding the selection forces governing genetic diversity in regulatory regions. By genome resequencing and modeling the effects of genetic variation in natural populations, we found that the evolutionary genetic signals of most regulatory elements were indeed consistent with them experiencing largely neutral evolution, not dissimilar to 4-fold neutral sites. The strongest evidence for purifying selection was observed for H3K27ac peaks assigned to UTRs (overlapping promoters and transcription start sites) and coding sequences, whereas intronic and intergenic H3K27ac peaks, most likely representing enhancer elements, appear evolving largely neutrally. The selection forces acting on these H3K27ac regions however did not differ from their sequence context in general, suggesting that the driving force behind different strengths of selection between H3K27ac peaks was not due to differences in their functionality, but rather their genomic context. Intriguingly, promoter elements show more conserved evolution across mammals as well, compared with enhancer elements (Villar et al. 2015; Berthelot et al. 2018). This suggests that similarly contrasting dynamics between promoter and enhancer elements observed between ohnologs following WGD are also manifested in interspecific regulatory evolution, and likely have similar causes stemming from different genomic contexts. Our results also imply that expression level divergence between ohnologs in the Atlantic salmon genome is presently without major selective effects at large. We anticipate that functional dissection of additional tissues, developmental time points as well as related species will eventually uncover additional evolutionary signatures on regulatory element divergence.

We additionally see that the Atlantic salmon genome has very few strongly deleterious variants ($N_es > 100$) in any genomic region in stark contrast to larger N_e species such as many plants (40–80% of coding SNPs with $N_es > 100$) (Gossmann et al. 2010), birds (~80% of 0-fold degenerate SNPs with $N_es > 10$ in the great tit and zebra finch) (Corcoran et al. 2017), insects (*Drosophila melanogaster* 78% of nonsynonomous SNPs with $N_es > 100$) (Kousathanas and Keightley 2013), or small mammals (*Mus musculus castaneus* 69% of nonsynonomous SNPs with $N_es > 100$) (Kousathanas and Keightley 2013). This suggests that the salmon N_e is currently reduced to the point where selection is unable to act efficiently on many variants, even in coding regions, where over 50% of nonsynonymous mutations seem to be effectively neutral or only weakly deleterious. Thus, any weak selection, such as may be expected at H3K27ac peaks, is likely swamped by genetic drift. However, this is not reflected by our α estimate of approximately 40% at 0-fold degenerate sites, which represents the proportion of fixations that are adaptive along the whole branch leading to Atlantic salmon from the salmon-brown trout (*Salmo trutta*) split. Together, these results suggest that from a longer term perspective, selection has been relatively efficient since the divergence of Atlantic salmon and brown trout.

Previous studies on gene expression evolution in salmonids support our conclusion that regulatory evolution in salmon follows a predominantly neutral pattern. Tissue expression divergence indicates that asymmetric evolution of expression levels dominates in salmonids (Lien et al. 2016), which is consistent with the largely neutral evolution of gene regulatory elements observed here. Contrasting results showing purifying selection on gene expression levels between salmonids have been reported as well (Varadharajan et al. 2018). Nevertheless, (Gillard et al. 2020) recently found significant evidence for predominant pseudogenization of expression levels (neutral loss of expression patterns) across salmonids. We have shown here that the most likely explanation for such predominant pattern of pseudogenization of expression patterns is likely coupled with largely neutral *cis*-regulatory evolution. Predominantly neutral evolution of regulatory sequences may also help explain the observed prevalence of pseudogenization of ohnologs in the absence of strong coding sequence divergence (Lien et al. 2016).

Our study demonstrates that an ancient WGD continues to have an impact on the regulatory landscape of the Atlantic salmon genome after at least 80 Myr of evolution. Overall, massive functional redundancy could potentially lift selective constraints on most gene regulatory elements, with a notable exception of gene promoters and coding sequences, which among regulatory elements showed the strongest signals of past selection. Genome-wide, the tempo of regulatory evolution has varied, with parts of the genome that experienced longer polyploidy showing less regulatory divergence. We anticipate that future studies will uncover selected regulatory elements within this largely neutrally evolving post-WGD regulatory genome.

Materials and Methods

Experimental Design and Collection of Material

We collected immature male gonads from five 11- to 12-month-old male Atlantic salmon raised in common-garden conditions (see details in Verta et al. [2020]). Fish were euthanized using an overdose of MS-222, followed by decapitation. Gonads were dissected under a microscope, flash-frozen in liquid nitrogen, and stored in −80 °C until use for chromatin extraction.

H3K27ac ChIPmentation

We integrated the original ChIPmentation protocol (Schmidl et al. 2015) to the workflow from ThermoFisher MAGnify ChIP kit. Gonads were homogenized in D-PBS buffer using OMNI Beadruptor Elite device in 2 ml tubes and 2.8 mm stainless steel beads. Chromatin was fixed using 1% formaldehyde for 2 min, followed by quenching using 0.125 M glycerine concentration for 5 min. Cells were collected using centrifugation and resuspended in lysis buffer supplemented with protease inhibitors. Chromatin was sheared in 150 μl volumes using a Bioruptor device with settings high power and 3x eight cycles of 30 s on, 30 s off. Debris was pelleted by centrifugation and sheared chromatin was diluted to IP conditions. An aliquot of sheared chromatin was reserved as input control. Acetylated histones were immunoprecipitated in +4 degrees C for 2 h using 1 μg of Abcam ab4729 on ThermoFisher Dynabeads Protein A/G. Beads were subsequently washed following MAGnify kit protocol, with an additional final wash using 10 mM Tris (pH 8). Bead-bound chromatin was then treated with a tagmentation reaction containing Illumina Tn5 transposase for 5 min at 37 degrees C. Tagmentation was terminated by adding 7.5 volumes of RIPA buffer and incubation on ice for 5 min. ChIPmented chromatin was subsequently washed twice with both RIPA and TE buffer. Crosslinks were reversed using a proteinase-K treatment and ChIPment DNA was captured using magnetic beads. These steps were performed following the MAGnify kit protocol (for three samples), or alternatively by using a reverse crosslinking buffer (10 mM Tris–HCl pH8, 0.5% SDS, 300 mM NaCl, 5 mM EDTA, proteinase-K) and Macherey-Nagel NucleoMag magnetic beads (for two samples). Input controls were treated with tagmentation reaction for 5 min at 55 degrees C. Tn5 was inactivated by adding SDS and tagment DNA was purified using Macherey-Nagel NucleoMag magnetic beads. Successful adapter integration was tested using PCR and primers aligning with Nextera adapters.

Alignment of ChIP-Seq Reads

ChIPmentation and matched input control libraries were sequenced using Illumina Nextseq chemistry at the Institute of Biotechnology of the University of Helsinki. Libraries were sequenced using both single-end and paired-end strategies, and the resulting ChIP fragment directories combined for each sample as described in the following section. For single-end libraries, reads were passed through a quality-control including Nextera adapter trimming using *fastp* (Chen et al. 2018) and the following parameters *–low_complexity_filter –trim_tail1 = 1 –trim_front1 = 19*. Reads were then aligned to the Atlantic salmon genome (Lien et al. 2016) downloaded from NCBI (version: ICSASG_v2, available from: ftp://ftp.ncbi.nlm.nih.gov/genomes/all/GCF/000/233/375/GCF_000233375.1_ICSASG_v2/GCF_000233375.1_ICSASG_v2_genomic.fna.gz) using *bowtie2 v2.4.2* (Langmead and Salzberg 2012) and the following parameters *–very-sensitive –end-to-end*. Paired-end libraries were correspondingly analyzed using *fastp* (*–low_complexity_filter –trim_front1 = 19 –trim_tail1 = 50 –trim_tail2 = 12*) and *bowtie2* (*–very-sensitive –maxins 1500 –end-to-end*). Alignment files were then quality filtered using *samtools* (Li et al. 2009) and parameters *-F 256 -q 20*.

Identification and Annotation of H3K27ac Peaks

We used *HOMER* (Heinz et al. 2010) to call enriched H3K27ac regions over input control and to annotate the reproducible peaks. ChIP fragment distributions were created using the command *makeTagDirectory* and parameters *-keepOne -single -tbp 1 -mis 5 -GCnorm default*. Tag directories for single-end and paired-end libraries for the same samples were then combined similarly with a *makeTagDirectory* command. Reproducible H3K27ac regions were identified with the command *getDifferentialPeaksReplicates.pl*, specifying parameters *-style histone*. Results were transformed into a bed file with *pos2bed.pl*. We then used custom *R* (R Core Team 2013) code and *bedtools intersect* (Quinlan and Hall 2010) to filter the peaks for any overlapping 1-kb genomic windows with the top 1% of mean sequencing coverage to avoid problematic regions of the genome. Peaks were then assigned to closest TSS's in the NCBI gene models (ICSASG_v2) and annotated using a *annotatePeaks.pl* command and parameters *-CpG*, which resulted in peaks annotated based on the peak center overlap with gene models as "promoter-TSS" (−1,000 to +100 bp relative to TSS), "intron," "exon," "transcription end-site (TES)," and "intergenic." Transcription factor binding-motif search was performed using *findMotifsGenome.pl* and parameters *-size given*. Finally, specific instances of motifs and their coverage were identified using *annotatePeaks.pl* and parameters *-m*, and parameters *-size 4000 -hist 10 -m -d*.

RNA-Seq Alignment and Quantification

RNA-seq reads of immature male gonads (SRR8479243, SRR8479245, SRR8479246) (Skaftnesmo et al. 2017) as well as 14 salmon tissues from Lien et al. (2016) were downloaded from *Sequence Read Archive* and filtered using *fastp* and default parameters. We used *STAR* (Dobin et al. 2013) to create a genome index (*-runMode genomeGenerate*) and align RNA-seq reads to the Atlantic salmon genome downloaded from *NCBI*, in manual two-pass mode, with the following parameters—*outFilterIntronMotifs Remove NoncanonicalUnannotated –chimSegmentMin 10 –outFilterT* *ype BySJout –alignSJDBoverhangMin 1 –alignIntronMin 20 –alignIntronMax 1000000 –alignMatesGapMax 1000000 –quantMode GeneCounts –alignEndsProtrude 10 Concordant Pair—limitOutSJcollapsed 5000000*. Alignments were quantified over gene models downloaded from *NCBI* using *R* function *featurecounts* from the *Rsubread* package (Liao et al. 2019) and normalized using *DESeq2 varianceStabilizing Normalization* (Love et al. 2014) (immature male gonads) or RPKM (14 tissues). The set of 14 tissues reported in Lien et al. (2016) was used for the analysis in supplementary figure S1, Supplementary Material online, whereas the set of immature testes expression reported in Skaftnesmo et al. (2017) was used for all other analyses.

Analysis of Population Resequencing Data

Read Mapping

We downloaded the raw reads for the whole-genome resequencing data set described in Barson et al. (2015) from the European Nucleotide Archive (ENA) under study accession number PRJEB10744 (available from: https://www.ebi.ac.uk/ena/browser/view/PRJEB10744). The data set comprises 31 salmon individuals from seven populations across the Atlantic and Barents Sea sequenced using the Illumina HiSeq 2500 platform (125 bp, paired end reads).

We cleaned the reads and removed adapter contamination using *Trim Galore* (version: 0.6.4_dev) (available from: https://github.com/FelixKrueger/TrimGalore) with *Cutadapt* (version: 2.7) (Martin 2011). We then aligned the reads to Atlantic salmon reference genome using *BWA-MEM* (version: 0.7.17-r1188) (Li 2013) and marked PCR duplicates and added read group information using *Picard* (version: 2.22.4) (Institute, https://broadinstitute.github.io/picard/). This resulted in a mean mapped coverage of 8× (see supplementary table S1, Supplementary Material online, for individual sample coverages).

Variant Calling

We followed the GATK (version: 4.1.3.0) pipeline to call SNPs (Auwera et al. 2013), and restricted our data set to assembled chromosomes only. First, we generated a training set for use in base quality score recalibration (BQSR) and variant quality score recalibration (VQSR) by intersecting an initial SNP call set obtained using *HaplotypeCaller* and *GenotypeGVCF* in GATK with a call set obtained using *SAMtools* (version: 1.9). We further subset the training set by intersecting it with the positions of variants used on the 20k and 200k salmon SNP chips. Second, we performed BQSR using this training set to produce recalibrated BAM files. Third, we called SNPs from the recalibrated BAM files using *HaplotypeCaller* and *GenotypeGVCF* in GATK. Forth, we performed VQSR, retaining variants that passed a tranche level cut-off of 99.5%. Finally, we filtered out SNPs that were multiallelic, fell in repetitive regions, had a mean depth below 4× or above 16× (half and twice the mean coverage) and that were missing genotype calls in some individuals. This resulted in a data set of 3,723,849 SNPs.

Whole-Genome Alignment and Ancestral States

To infer the ancestral alleles of the SNPs in our data set, we used a 9-way multispecies whole-genome alignment and maximum parsimony using the brown trout (*Salmo trutta*) Atlantic salmon (*Salmo salar*), Arctic charr (*Salvelinus alpinus*) sequences; at each biallelic SNP in salmon, to assign an allele as ancestral, we required it matched the sequence in the other two species. This resulted ancestral alleles inferred for 1,614,400 out of 3,723,849 SNPs.

The whole-genome alignment was performed as follows. Pairwise alignments were generated between each brown trout chromosome and each query species genome (a full list of species and genome versions can be seen in supplementary table S3, Supplementary Material online) using *LASTZ* (Harris 2007). The pairwise chromosomal alignments were then chained using *axtChain* and netted with *chainNet* (Kent et al. 2003) The chromosomal alignments were merged into whole-genome alignments and single coverage was insured for the reference sequence (the brown trout reference genome) using *single_cov2.v11* from the *MULTIZ* package (Blanchette et al. 2004). *MULTIZ* was then used to align the pairwise alignments using the automation script *roast*.

Annotating Variants

We identified SNPs falling in different genomic regions (intergenic, intronic, untranslated regions [UTRs], coding sequence [CDS]) by creating bed files of their coordinates from the NCBI GFF file for version CSASG_v2 of the Atlantic salmon genome (available from: ftp://ftp.ncbi.nlm.nih.gov/genomes/all/GCF/000/233/375/GCF_000233375.1_ICSASG_v2/GCF_000233375.1_ICSASG_v2_genomic.gff.gz). To obtain genomic coordinates for 4-fold degenerate sites, we parsed the CDS fasta file for the same genomic version (available from: ftp://ftp.ncbi.nlm.nih.gov/genomes/all/GCF/000/233/375/GCF_000233375.1_ICSASG_v2/GCF_000233375.1_ICSASG_v2_cds_from_genomic.fna.gz) with a custom python script. Finally, we obtained coordinates for repeat regions in the genome from the repeat masker output from NCBI (available from: ftp://ftp.ncbi.nlm.nih.gov/genomes/all/GCF/000/233/375/GCF_000233375.1_ICSASG_v2/GCF_000233375.1_ICSASG_v2_rm.out.gz).

Summary Statistics

We calculated nucleotide diversity (π, Tajima 1983) and Tajima's *D* (Tajima 1989) for CDS sites, 4-fold degenerate sites, UTRs, introns as well as sites within enhancers, subdivided by their genomic location (intergenic, intronic, and UTRs). To extract variants within these regions, we intersected our VCF file with the relevant BED file generated from our annotation pipeline, using *BEDTools* (version: 2.26.0).

To obtain per site estimates of π, we created a custom FASTA file containing all sites in the genome that passed our variant calling filters (see Variant Calling above), by applying the filters to an all sites (monomorphic sites and variants) VCF file output during variant calling, from GATK's *HaplotypeCaller* with the *-ERC GVCF* flag. From this file, we calculated the number of callable sites for each genomic region.

Distribution of Fitness Effects

We estimated the distribution of fitness effects (DFE) using the package *anavar* (version 1.2) (Barton and Zeng 2018). Briefly, the method uses the site frequency spectrum to estimate the population scaled mutation rate ($\theta = 4N_e\mu$) and shape and scale parameters for a gamma distribution of population scaled selection coefficients ($\gamma = 4N_es$). Here, we present the gamma distributions as the proportion of variants falling into four selective bins, effectively neutral ($0 \leqslant N_es \leqslant 1$), weakly deleterious ($1 < N_es \leqslant 10$), deleterious ($10 < N_es \leqslant 100$), and strongly deleterious ($N_es > 100$).

We fitted the *neutralSNP_vs_selectedSNP* model, with a continuous gamma distribution to model the strength of selection, separately to CDS sites, UTRs, introns, and sites within enhancers, subdivided by their genomic location (intergenic, intronic, and UTRs). The model takes the unfolded site frequency spectrum for a focal set of sites and estimates the population scaled mutation rate ($\theta = 4N_e\mu$, where N_e is the effective population size and μ is the per site per generation mutation rate), the shape and scale parameters for a gamma distribution of population scaled selection coefficients ($\gamma = 4N_es$, where s is the selection coefficient), and the rate of ancestral state misidentification (polarization error; ε), which is used internally to correct the SFS. The model also uses the site frequency spectrum from a putatively neutral set of sites to control for the confounding effects of demography following the method of Eyre-Walker et al. (2006). Here, we used the SFS from 4-fold degenerate sites for this purpose. We present our DFE results by using the estimated gamma distribution of selection coefficients to estimate the proportion of variants falling into four γ bins (note all γ estimates are negative), effectively neutral ($0 \leqslant \gamma \leqslant 1$), weakly deleterious ($1 < \gamma \leqslant 10$), deleterious ($10 < \gamma \leqslant 100$), and strongly deleterious ($\gamma > 100$).

Bootstrapping

To obtain 95% confidence intervals for our summary statistics and DFE analyses, we performed 100 rounds of resampling with replacement by gene for each SFS data set. That is, for a given focal SFS, we resampled both the focal SFS and the neutral reference SFS (4-fold degenerate sites) and the number of callable sites for each per gene. We then recalculated π and Tajima's *D*, and re-estimated the DFE for each bootstrap replicate.

Calculating α

In order to calculate the proportion of substitutions fixed by positive selection (α), we first obtained divergence estimates for each genomic region in the DFE analyses and for 4-fold degenerate sites. To that end, we created concatenated FASTA alignments for each region, using the Atlantic salmon, Arctic charr, and brown trout sequences in our whole-genome alignment. We then used the APE package (version 5.4.1) (Paradis et al. 2004) in R (version 3.5.1) to estimate the pairwise distance matrix between species using *dist.dna* with the *K80* model, which we then used to calculate divergence on the Atlantic salmon branch since its split from brown trout.

Second, we estimated the fixation probabilities for deleterious mutations ($\bar{\mu}$) in each genomic region using our DFE estimates with:

$$\int_0^\infty \frac{-\gamma\ f(\gamma|a,\ b)}{1-e^{-\gamma}}\, d\gamma,$$

where $f(\gamma|a,\ b)$ is the probability density function of the reflected Γ distribution of fitness effects, with a the shape parameter and b the scale parameter, as estimated by *anavar*.

Finally, we substituted $\bar{\mu}$ into (equation 19 from Barton and Zeng [2018]):

$$\alpha = \frac{d_N - d_S\bar{\mu}}{d_N},$$

Where d_N is our divergence estimate for our focal sites from the DFE analysis and d_S is the divergence estimate for 4-fold degenerate sites (our neutral reference).

Downstream Analyses

We identified ohnologs using best reciprocal BlastP matches and corresponding homeoblock localization (Lien et al. 2016) using a custom *Python 3* script. Briefly, we selected the longest transcript for all gene models using the *primary_transcript.py* script in *Orthofinder* (Emms and Kelly 2015). Using *Python 3*, we then ran BlastP of all primary transcripts against each other, identifying those that showed best reciprocal matches. Genes corresponding to these transcripts that were situated in corresponding homeoblocks as defined in Lien et al. (2016) were designated as ohnologs. All subsequent analyses were performed with custom scripts in *R* (*Dryad* DOI: https://doi.org/10.5061/dryad.t4b8gtj1b).

Supplementary Material

Supplementary data are available at *Genome Biology and Evolution* online.

Acknowledgments

This work was supported by the European Research Council (Grant Agreement No. 742312), Academy of Finland (Grant Nos. 314254 and 314255), and the University of Helsinki. We thank the Primmer lab members for help in fish husbandry and sampling, staff from the Natural Resources Institute Finland (Luke) Taivalkoski hatchery for assistance with the initial salmon crosses, Kai Zeng for providing example code to calculate alpha, and CSC—IT Center for Science, Finland, for computational resources.

Data Availability

For the resequencing data preparation and subsequent analysis, all scripts and command lines are available on GitHub (available from: https://github.com/henryjuho/sal_enhancers). Preprocessed ChIPmentation data and associated *R* scripts are available at the Dryad repository (DOI: https://doi.org/10.5061/dryad.t4b8gtj1b). ChIPmentation raw data are available through the Sequence Read Archive (Supplementary table 1).

Literature Cited

Andersson R, Sandelin A. 2019. Determinants of enhancer and promoter activities of regulatory elements. Nat Rev Genet. 337:1190–1117.

Auwera GD, et al. 2013. From FastQ data to high confidence variant calls: the Genome Analysis Toolkit best practices pipeline. Curr Protoc Bioinformatics. 43:11.10.1–33.

Baron D, Houlgatte R, Fostier A, Guiguen Y. 2005. Large-scale temporal gene expression profiling during gonadal differentiation and early gametogenesis in rainbow Trout1. Biol Reprod. 73(5):959–966.

Barson NJ, et al. 2015. Sex-dependent dominance at a single locus maintains variation in age at maturity in salmon. Nature 528(7582):405–408.

Barton HJ, Zeng K. 2018. New methods for inferring the distribution of fitness effects for INDELs and SNPs. Mol Biol Evol. 35(6):1536–1546.

Berthelot C, Villar D, Horvath JE, Odom DT, Flicek P. 2018. Complexity and conservation of regulatory landscapes underlie evolutionary resilience of mammalian gene expression. Nat Ecol Evol. 2(1):152–163.

Blanchette M, et al. 2004. Aligning multiple genomic sequences with the threaded blockset aligner. Genome Res. 14(4):708–715.

Cao Q, et al. 2017. Reconstruction of enhancer–target networks in 935 samples of human primary cells, tissues and cell lines. Nat Genet. 49(10):1428–1436.

Chen S, Zhou Y, Chen Y, Gu J. 2018. fastp: an ultra-fast all-in-one FASTQ preprocessor. Bioinformatics 34(17):i884–i890.

Corcoran P, Gossmann TI, Barton HJ, Slate J, Zeng K. 2017. Determinants of the efficacy of natural selection on coding and noncoding variability in two passerine species. Genome Biol Evol. 9(11):2987–3007.

Creyghton MP, et al. 2010. Histone H3K27ac separates active from poised enhancers and predicts developmental state. Proc Natl Acad Sci U S A. 107(50):21931–21936.

Dehal P, Boore JL. 2005. Two rounds of whole genome duplication in the ancestral vertebrate. PLoS Biol. 3(10):e314.

Dobin A, et al. 2013. STAR: ultrafast universal RNA-seq aligner. Bioinformatics 29(1):15–21.

Elurbe DM, et al. 2017. Regulatory remodeling in the allo-tetraploid frog *Xenopus laevis*. Genome Biol. 18(1):198.

Emms DM, Kelly S. 2015. OrthoFinder: solving fundamental biases in whole genome comparisons dramatically improves orthogroup inference accuracy. Genome Biol. 16:157.

Eyre-Walker A, Woolfit M, Phelps T. 2006. The distribution of fitness effects of new deleterious amino acid mutations in humans. Genetics 173(2):891–900.

Gasperini M, Tome JM, Shendure J. 2020. Towards a comprehensive catalogue of validated and target-linked human enhancers. Nat Rev Genet. 21(5):292–319.

Gillard GB, et al. 2020. Comparative regulomics reveals pervasive selection on gene dosage following whole genome duplication. *Biorxiv*:2020.07.20.212316; doi: 10.1101/2020.07.20.212316.

Gossmann TI, et al. 2010. Genome wide analyses reveal little evidence for adaptive evolution in many plant species. Mol Biol Evol. 27(8):1822–1832.

Hallin J, Landry CR. 2019. Regulation plays a multifaceted role in the retention of gene duplicates. PLoS Biol. 17(11):e3000519.

Harris RS. 2007. Improved pairwise alignment of genomic DNA. University Park (PA): The Pennsylvania State University.

Heinz S, et al. 2010. Simple combinations of lineage-determining transcription factors prime cis-regulatory elements required for macrophage and B cell identities. Mol Cell. 38(4):576–589.

Jiang C, Pugh BF. 2009. Nucleosome positioning and gene regulation: advances through genomics. Nat Rev Genet. 10(3):161–172.

Kent WJ, Baertsch R, Hinrichs A, Miller W, Haussler D. 2003. Evolution's cauldron: duplication, deletion, and rearrangement in the mouse and human genomes. Proc Natl Acad Sci U S A. 100(20):11484–11489.

King MC, Wilson AC. 1975. Evolution at two levels in humans and chimpanzees. Science 188(4184):107–116.

Kousathanas A, Keightley PD. 2013. A comparison of models to infer the distribution of fitness effects of new mutations. Genetics 193(4):1197–1208.

Langmead B, Salzberg SL. 2012. Fast gapped-read alignment with Bowtie 2. Nat Methods. 9(4):357–359.

Li H. 2013. Aligning sequence reads, clone sequences and assembly contigs with BWA-MEM. *Arxiv*:1303.3997.

Li H, et al. 2009. The Sequence Alignment/Map format and SAMtools. Bioinformatics 25(16):2078–2079.

Liao Y, Smyth GK, Shi W. 2019. The R package Rsubread is easier, faster, cheaper and better for alignment and quantification of RNA sequencing reads. Nucleic Acids Res. 47:gkz114.

Lien S, et al. 2016. The Atlantic salmon genome provides insights into rediploidization. Nature 533(7602):200–205.

Liu Z, et al. 2007. Molecular cloning of doublesex and mab-3-related transcription factor 1, forkhead transcription factor gene 2, and two types of cytochrome P450 aromatase in Southern catfish and their possible roles in sex differentiation. J Endocrinol. 194(1):223–241.

Long HK, Prescott SL, Wysocka J. 2016. Ever-changing landscapes: transcriptional enhancers in development and evolution. Cell 167(5):1170–1187.

Love MI, Huber W, Anders S. 2014. Moderated estimation of fold change and dispersion for RNA-seq data with DESeq2. Genome Biol . 15(12):550.

Macqueen DJ, Johnston IA. 2014. A well-constrained estimate for the timing of the salmonid whole genome duplication reveals major decoupling from species diversification. Proc Biol Sci. 281(1778):20132881.

Macqueen DJ, et al. 2017. Functional Annotation of All Salmonid Genomes (FAASG): an international initiative supporting future salmonid research, conservation and aquaculture. BMC Genomics 18(1):484.

Martin M. 2011. Cutadapt removes adapter sequences from high-throughput sequencing reads. EMBnet J. 17(1):10–12.

Mavrich TN, et al. 2008. A barrier nucleosome model for statistical positioning of nucleosomes throughout the yeast genome. Genome Res. 18(7):1073–1083.

Paradis E, Claude J, Strimmer K. 2004. APE: analyses of phylogenetics and evolution in R language. Bioinformatics 20(2):289–290.

Peer Y. D, Maere S, Meyer A. 2009. The evolutionary significance of ancient genome duplications. Nat Rev Genet. 10(10):725–732.

Pfennig F, Standke A, Gutzeit HO. 2015. The role of Amh signaling in teleost fish – multiple functions not restricted to the gonads. Gen Comp Endocrinol. 223:87–107.

Quinlan AR, Hall IM. 2010. BEDTools: a flexible suite of utilities for comparing genomic features. Bioinformatics 26(6):841–842.

R Core Team. 2013. R: a language and environment for statistical computing. Vienna, Austria: R Foundation for Statistical Computing.

Robertson FM, et al. 2017. Lineage-specific rediploidization is a mechanism to explain time-lags between genome duplication and evolutionary diversification. Genome Biol. 18(1):111.

Sacerdot C, Louis A, Bon C, Berthelot C, Crollius HR. 2018. Chromosome evolution at the origin of the ancestral vertebrate genome. Genome Biol. 19(1):166.

Sandra G-E, Norma M-M. 2010. Sexual determination and differentiation in teleost fish. Rev Fish Biol Fisheries. 20(1):101–121.

Schmidl C, Rendeiro AF, Sheffield NC, Bock C. 2015. ChIPmentation: fast, robust, low-input ChIP-seq for histones and transcription factors. Nat Methods. 12(10):963–965.

Skaftnesmo KO, et al. 2017. Integrative testis transcriptome analysis reveals differentially expressed miRNAs and their mRNA targets during early puberty in Atlantic salmon. BMC Genomics 18(1):801.

Skene PJ, Henikoff S. 2015. A simple method for generating high-resolution maps of genome-wide protein binding. Elife 4:e09225.

Stern DL, Orgogozo V. 2008. The loci of evolution: how predictable is genetic evolution? Evolution 62(9):2155–2177.

Tajima F. 1983. Evolutionary relationship of DNA sequences in finite populations. Genetics 105(2):437–460.

Tajima F. 1989. Statistical method for testing the neutral mutation hypothesis by DNA polymorphism. Genetics 123(3):585–595.

Vandepoele K, et al. 2004. Major events in the genome evolution of vertebrates: paranome age and size differ considerably between ray-finned fishes and land vertebrates. Proc Natl Acad Sci U S A. 101(6):1638–1643.

Varadharajan S, et al. 2018. The Grayling genome reveals selection on gene expression regulation after whole-genome duplication. Genome Biol Evol. 10(10):2785–2800.

Verta J-P, et al. 2020. Cis-regulatory differences in isoform expression associate with life history strategy variation in Atlantic salmon. PLoS Genet. 16(9):e1009055.

Viger RS, Guittot SM, Anttonen M, Wilson DB, Heikinheimo M. 2008. Role of the GATA family of transcription factors in endocrine development, function, and disease. Mol Endocrinol. 22(4):781–798.

Villar D, et al. 2015. Enhancer evolution across 20 mammalian species. Cell 160(3):554–566.

Villar D, Flicek P, Odom DT. 2014. Evolution of transcription factor binding in metazoans – mechanisms and functional implications. Nat Rev Genet. 15(4):221–233.

Wu X, et al. 2010. The POU domain transcription factor POU3F1 is an important intrinsic regulator of GDNF-induced survival and self-renewal of mouse spermatogonial stem cells. Biol Reprod. 82(6):1103–1111.

Associate editor: Soojin Yi